

# Real-Time Heuristic Motion Planning for Autonomous Vehicle Driving

Shyr-Long Jeng \*, Wei-Hua Chieng \*\* and Yung-Chen Wang \*\*\*

**Keywords :** path planning, autonomous vehicle, heuristic

## ABSTRACT

This study presents a novel method that can be used to perform dynamic motion planning for a nonholonomic four-wheeler vehicle according to actual dynamic constraints to achieve a rapid response in the driving environment and obtain optimal vehicle performance. The proposed intuitive steering model employs inferential heuristics of driving behavior and relevant two-direction indices obtained from a driver's-perspective view instead of traditional path planning to quickly and efficiently generate target paths without the requirement of complicated mathematical calculations. In the full model of a nonholonomic vehicle, a chassis with Ackerman steering geometry and double-wishbone suspension, lateral and longitudinal forces from contact strains, and forces due to the suspension system are considered to verify the motion of an autonomous vehicle from its starting position to its destination. Simulations of lane changes and U-turn maneuvers reveal that the proposed method provides a feasible trajectory in real time. The path planning method is effective for many driving scenarios, provides high dynamic performance, and maintains high maneuverability. This method is intuitive and extensible, thus allowing vehicles to navigate in real time and adapt to dynamic environmental conditions.

## INTRODUCTION

Autonomous vehicles and advanced driver assistance systems improve transportation safety and comfort. Path planning is a key and challenging task in autonomous driving. Autonomous decision-making

systems process observation data streams from onboard sensors such as radars, light detection and ranging systems, cameras, global positioning system or inertial navigation system units, and odometers. A perception system employs a priori information and collected observation data to evaluate the state of an autonomous vehicle and its surrounding environment. Then, the decision system conducts an estimation to control the vehicle for reaching the required destination. The vehicle moves in various environments by performing different action sequences. Real-time motion planning with efficient navigation is critical to the successful use of autonomous vehicles.

Various types of intelligent algorithms are available for path planning, navigation, and the tracking of autonomous vehicles (Zhu *et al.*, 2019; González *et al.*, 2015). Dijkstra's algorithm (Dijkstra 1959) searches for the shortest path from a source node to a target node in a map with a single source. The algorithm wastes time exploring in directions that are not promising. The A\* algorithm (Cai *et al.*, 2014; Dolgov *et al.*, 2010; Soltani *et al.*, 2002) considers the actual distance from the starting point and the estimated distance to the destination. Compared with traditional methods, such as neural networks, genetic algorithms, fuzzy logic algorithms, and ant colony optimization (Kuwata *et al.*, 2019), the aforementioned two heuristic approaches are more intelligent and advanced for dealing with complex problems. However, these algorithms construct a directed graph to uniformly sample the configuration space and randomly explore the free space of the environment at runtime.

Vehicle dynamics modeling systems (Chen, *et al.*, 2018; Tavan *et al.*, 2015) have been used to track or improve maneuverability and stability of vehicles over a desired path. The longitudinal force and sideslip angle are crucial factors for the lateral stability and path-following motion of vehicles. The vehicle model applies a corrected steering angle and torque on the wheels to maintain the vehicle on the required trajectory while modifying its handling. By simulating of lane changes and U-turn scenarios, the influence of various maneuvering operations on the longitudinal and lateral dynamic performance of the vehicle can be studied.

*Author for Correspondence: Shyr-Long Jeng.*

\* Associate Professor, Department of Mechanical Engineering  
Lunghwa University of Science and Technology, Taiwan, R.O.C.

\*\* Professor, Department of Mechanical Engineering National  
Chiao Tung University, Taiwan, R.O.C

\*\*\* Researcher, Electric Propulsion and Control Department,  
Industrial Technology Research Institute, Taiwan, R.O.C

## HEURISTIC RULES FOR PATH PLANNING

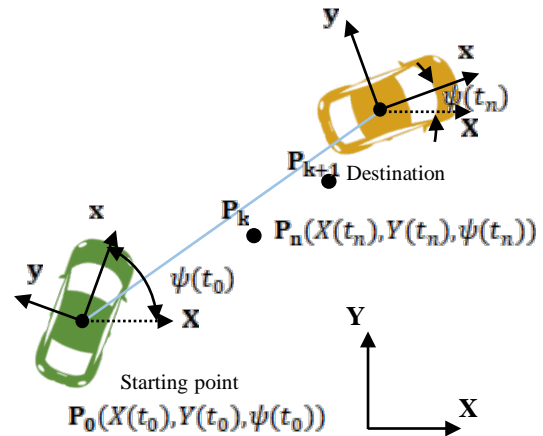
Figure 1 displays a vehicle path from the starting point to the destination point on a planar surface. The global inertial and local body coordinate frames are denoted by  $X$ - $Y$ - $Z$  and  $x$ - $y$ - $z$ , respectively. The origin of the local coordinate frame is attached at the vehicle's center of gravity (COG). The  $x$ -axis points forward in the direction that the vehicle is facing. Moreover, the  $y$ -axis points to the left, as viewed when the vehicle is facing forward. The  $z$ -axis points upward, that is, perpendicular to the ground, to maintain a right-hand coordinate system. Each axis is positive in the counterclockwise direction, when looking in the positive direction of that axis. Rotation around the  $x$ -axis is known as roll ( $\theta$ ), rotation around the  $y$ -axis is called pitch ( $\phi$ ), and rotation around the  $z$ -axis is called yaw ( $\psi$ ).

Path planning is scheduled at regular intervals. During each planning cycle, a path planner generates paths from the current location with a look-ahead distance based on the speed and line-of-sight details obtained from the vehicle's onboard sensors. Moreover, each path is evaluated with respect to the destination position to determine the feasible path. The trajectory may be described as a sequence of states visited by the vehicle and is represented by  $P = (P_0, \dots, P_n)$  for  $n + 1$  nodes. Each node  $P_k$  described by the position vector at time  $t_k$  pertains to the real-time planning of the actual transition of the vehicle from one feasible state to the next, satisfying the vehicle's kinematic limits based on vehicle dynamics and constraining the navigation feasibility. Fig. 1(a) displays the trajectory of a vehicle traveling from the starting point  $P_0(X(t_0), Y(t_0), \psi(t_0))$  at time  $t_0$  to the destination point  $P_n(X(t_n), Y(t_n), \psi(t_n))$  at time  $t_n$ . The location parameters include the position  $(X, Y)$  and heading yaw angle  $\psi$  in the Cartesian coordinate system.

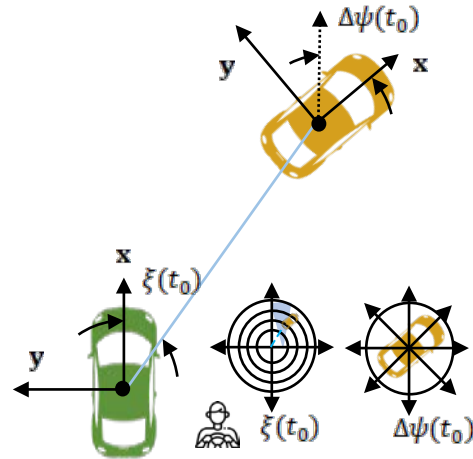
The vehicle movement is controlled by a series of independent driving behavior patterns. The decision system of the vehicle selects the paths from the current configuration to a given termination configuration based on the tactical maneuvering decision of the driver under different driving conditions. Fig. 1(b) illustrates the relationship between the position and orientation of the vehicle at the target point from the driver's-perspective view. The target angle  $\xi(t_0)$  and alignment angle  $\Delta\psi(t_0)$  are defined as follows at time  $t_0$ :

$$\xi(t_0) = \tan^{-1} \left( \frac{Y(t_n) - Y(t_0)}{X(t_n) - X(t_0)} \right) - \psi(t_0) \quad (1.a)$$

$$\Delta\psi(t_0) = \psi(t_n) - \psi(t_0) \quad (1.b)$$



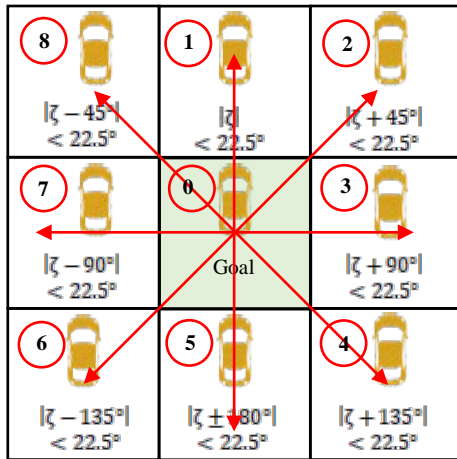
(a) Vehicle path with a global coordinate frame.



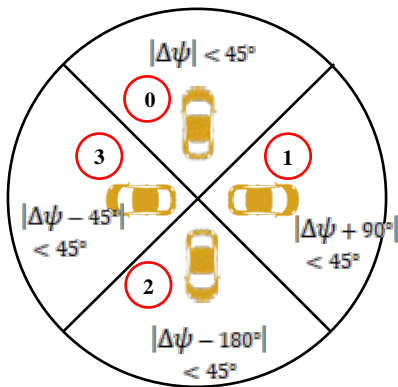
(b) Vehicle path with a local coordinate frame.

Fig. 1. Vehicle path toward the destination.

The target angle  $\xi$  is the relative angle between the target and current positions with respect to the local coordinate frame obtained from the vehicle being observed. The alignment angle  $\Delta\psi$  indicates the relative heading direction and determines whether the vehicle is aligned in the preset heading direction at the destination. To reduce the complexity of the heuristic rules, the target angle  $\xi$  is divided into eight regions by using a  $3 \times 3$  square grid. Fig. 2(a) displays the angular distribution of eight standard directions in the grid map, which provides a clear idea regarding the direction of the current node relative to the destination node. The vertically upward direction is set to  $0^\circ$ , and the counterclockwise direction is the positive direction. Eight cases of the destination direction exist in the grid map. The target angle range allowed for each grid is approximately  $45^\circ$ . A supplementary case of the central square is considered when the vehicle enters the area near the



(a) Target angle encode.



(b) Alignment angle encode.

Note: Note: The number inside the red circle indicates the code number.

Fig. 2. Two-angle index encode.

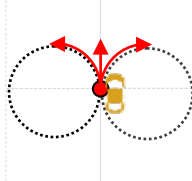
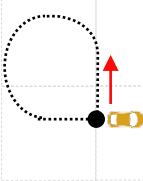
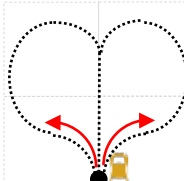
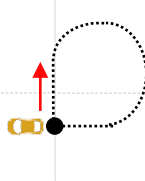
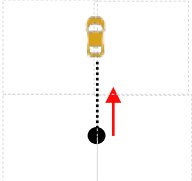
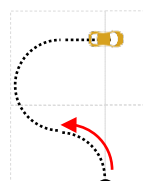
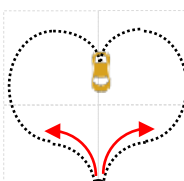
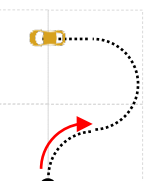
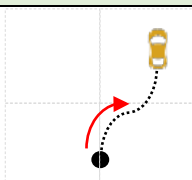
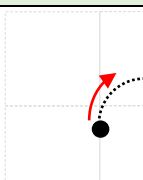
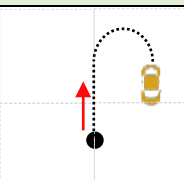
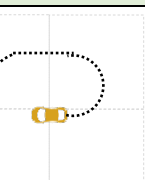
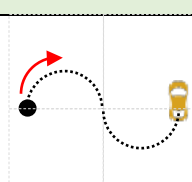
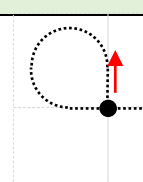
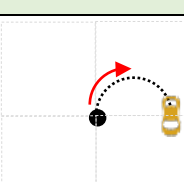
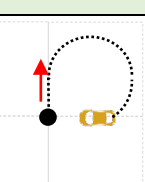
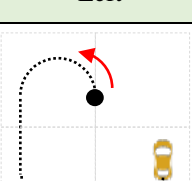
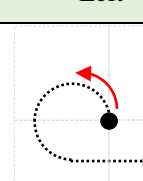
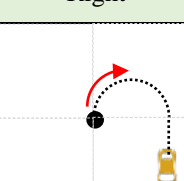
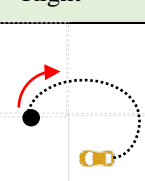
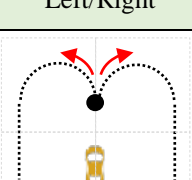
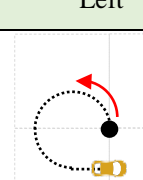
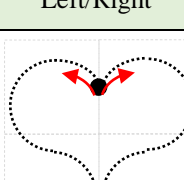
target zone. In total, nine regions are observed. These regions are encoded from zero to eight. Similar to the target angle  $\xi$ , the linguistic terms associated with the alignment angle  $\Delta\psi$  are set as follows: Ahead, Right, Behind, and Left. Each direction is at  $90^\circ$  from the following section, as illustrated in Fig. 2(b). We defined four regions, which are numbered from zero to three. These regions cover the complete alignment angle. The coded numbers 0, 1, 2, and 3 represent the Ahead, Right, Behind, and Left areas, respectively.

Table 1 presents a matrix representation comprising output actions under different driving states. The rows and columns designate the relative position of the target by presenting the two indices pertaining to the target angle  $\xi$  and alignment angle  $\Delta\psi$ , respectively. The big black dot indicates the current position of the vehicle, and the picture of the brown car provides the car orientation at the target location. The red arrows illustrate the possible output driving strategies that can be used in the specified target navigation condition. The dotted curves indicate the intuitive planning of the driving path from the starting point to the target position.

There exist 36 ( $9 \times 4 = 36$ ) combinations of driving environment situations. These combinations can provide four types of driving behaviors as output—go straight, stop, turn right, and turn left. The steering actions are designed using heuristic rules to describe the general driving behavior and constitute the main concept of the proposed algorithm. For instance, the cell (1, 1) located at the first row and first column of the matrix table can be considered rule (0-0). When the car enters the target zone and the heading direction is consistent with the preset vehicle attitude, four possible driving output behaviors exist—stop, continue straight through the target zone, turn left, and turn right. When the “go straight” command is received by a vehicle, the steering module of the vehicle is initiated to rewind the steering wheel to the center position. The steering angle gradually approaches zero, and the vehicle direction is then maintained straight. The steering angle progressively increases and decreases when the “turn left” and “turn left” commands are generated by the path planer, respectively. The dashed lines indicate that the vehicle will turn by  $360^\circ$  in the counterclockwise or clockwise directions to enter the rear portion of the target area after performing a left or right turn and then enter the target area again. Cell (2, 4) is defined as rule (1-3). The destination of this cell is at the 12 o’clock position, and the alignment angle is approximately  $90^\circ$  to the left. Although the target area is located directly in front of the car, the preset heading direction of the vehicle differs from the current driving direction by  $90^\circ$ . The driving behavior of the car is to turn right, and then, the car is ready to perform a  $270^\circ$  turn in the counterclockwise direction to enter the target zone.

Table 1. Heuristic rules with the target angle  $\xi$  and alignment angle  $\Delta\psi$ .

	Alignment angle $\Delta\psi$	Ahead $ \Delta\psi  < 45^\circ$ <b>0</b>	Right $ \Delta\psi + 90^\circ  < 45^\circ$ <b>1</b>	Behind $ \Delta\psi - 180^\circ  < 45^\circ$ <b>2</b>	Left $ \Delta\psi - 90^\circ  < 45^\circ$ <b>3</b>
Target angle $\xi$					

<p>Centre (goal area)</p> <p>0</p>	<p>Straight/Stop Left/Right</p> 	<p>Straight</p> 	<p>Left/Right</p> 	<p>Straight</p> 
<p>Front (12:00 o'clock)</p> <p><math> \xi  &lt; 22.5^\circ</math></p> <p>1</p>	<p>Straight</p> 	<p>Left</p> 	<p>Left/Right</p> 	<p>Right</p> 
<p>Front-right (1:30 o'clock)</p> <p><math> \xi + 45^\circ  &lt; 22.5^\circ</math></p> <p>2</p>	<p>Right</p> 	<p>Right</p> 	<p>Straight</p> 	<p>Straight</p> 
<p>Right (3:00 o'clock)</p> <p><math> \xi + 90^\circ  &lt; 22.5^\circ</math></p> <p>3</p>	<p>Right</p> 	<p>Straight</p> 	<p>Right</p> 	<p>Straight</p> 
<p>Rear-right (4:30 o'clock)</p> <p><math> \xi + 135^\circ  &lt; 22.5^\circ</math></p> <p>4</p>	<p>Left</p> 	<p>Left</p> 	<p>Right</p> 	<p>Right</p> 
<p>Rear (6:00 o'clock)</p> <p><math> \xi + 180^\circ  &lt; 22.5^\circ</math></p> <p>5</p>	<p>Left/Right</p> 	<p>Left</p> 	<p>Left/Right</p> 	<p>Right</p> 
<p>Rear-left</p>	<p>Right</p>	<p>Left</p>	<p>Left</p>	<p>Right</p>

(7:30 o'clock) $ \xi - 135^\circ  < 22.5^\circ$ 6				
Left (9:00 o'clock) $ \xi - 90^\circ  < 22.5^\circ$ 7	Right	Straight	Left	Straight
Front-left (9:00 o'clock) $ \xi - 45^\circ  < 22.5^\circ$ 8	Right	Straight	Straight	Left

### Adjustment of the Perspective View Angle

Consider three target ranges of associations—long range, closed range, and short range. Figure 3 presents a schematic of the target ranges. The moving area near the target zone is known as the short range, whereas the area far away from the target zone is known as the long range. The area in the middle is known as the closed range. The size of the circle is directly related to the target range.

In the heuristic table, the trajectory state of the target is determined by the discrete target and discrete alignment angles. Observing targets in different target ranges and perspectives can affect the state changes. As the vehicle approaches the short-range area of the target, the angular resolution becomes coarser and the perspective angle of the driver's view becomes larger. This concept is highly related to the gray scale inversion phenomenon. This finding indicates that the target has one viewing side in which the heuristic states change suddenly after exceeding a specified viewing angle. The heuristic states change abruptly within a short-range area due to vehicle movement. However, the states at long-range area would do not change in the long-range area.

The divided area of the perspective angles is flexibly adjusted according to the three different target ranges to avoid sudden changes in the heuristic state and to stabilize the automatic path planning. When the speed of the car is high and the perspective view angle is large, it becomes difficult for the car to reach the required location and direction within the short range. According to the proposed algorithm, the

outer range, that is, the long range, can still track the target at high speed. However, the perspective view angle is decreased to make the car travel in a more stable and straight manner on the path that is far from the target. When the car enters the closed range, the perspective view angle of the car increases. Thus, an attempt is made to bring the car closer to the required direction. Finally, in the short range, the speed is decreased and the view angle range increases to the maximum value for quickly adjusting the car to the target direction and location in each step.

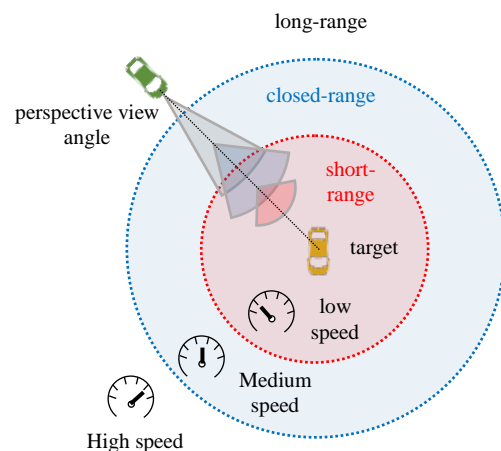


Fig. 3. Schematic of the vehicle under different target ranges.

### MODEL OF VEHICLE DYNAMICS

To simulate the vehicle's movement during various driving maneuvers, a full nonlinear vehicle model is proposed. This model includes the lateral and longitudinal dynamic characteristics specifically used for performing the driving and maneuvering behavior. Compared with the finite element method, our method provides a real-time numerical model for the dynamic analysis of the motion trajectory. Figure 4 displays a schematic of a four-wheeler vehicle model in the longitudinal, lateral, and yaw directions. The model comprises roll and pitch movements, wheel dynamics, and the coupling of longitudinal and lateral tire slips. The dynamics of the vehicle's center of mass are expressed as follows:

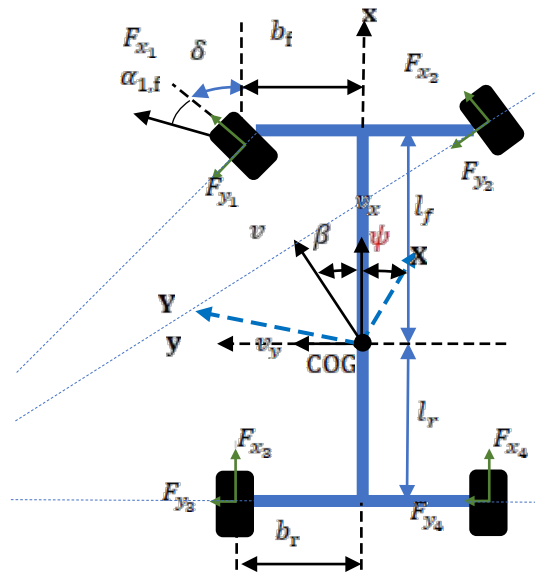


Fig. 4. Vehicle handling model.

$$\dot{X} = v_x \cos \psi - v_y \sin \psi \quad (2)$$

$$\dot{Y} = v_x \sin \psi + v_y \cos \psi \quad (3)$$

$$\dot{v}_x = \dot{\psi} v_y + \frac{1}{M_T} \left[ (F_{x1} + F_{x2}) \cos \delta - (F_{y1} + F_{y2}) \sin \delta + F_{x3} + F_{x4} \right] - F_{aero} \quad (4)$$

$$\dot{v}_y = -\dot{\psi} v_x + \frac{1}{M_T} \left[ (F_{x1} + F_{x2}) \sin \delta + (F_{y1} + F_{y2}) \cos \delta + F_{y3} + F_{y4} \right] \quad (5)$$

where  $X$  and  $Y$  are the longitudinal and lateral positions at the vehicle's COG with respect to the fixed inertial frame, respectively;  $v_x$  and  $v_y$  are the longitudinal and lateral speed of the vehicle, respectively;  $F_{x_j}$  and  $F_{y_j}$  ( $j = 1, 2, 3,$  and  $4$ ) are the longitudinal and lateral forces of the  $j$ th tire,

respectively;  $\delta$  is the steering angle of the front wheel;  $M_T$  is the total mass of the vehicle; and  $F_{aero}$  is the air drag force on the vehicle. The sideslip angle  $\beta$  of the vehicle's body at the COG is expressed as follows:

$$\beta \approx \tan^{-1} \left( \frac{v_y}{v_x} \right) \quad (6)$$

The yaw, roll, and pitch motions of the car's body are expressed as follows:

$$I_z \ddot{\psi} = l_f \left[ (F_{x1} + F_{x2}) \sin \delta + (F_{y1} + F_{y2}) \cos \delta \right] + l_r \left( -F_{y3} - F_{y4} \right) + b_f + b_r \left( -F_{x3} + F_{x4} \right) \quad (7)$$

$$I_x \ddot{\phi} = b_f (F_{z1} - F_{z2}) + b_r (F_{z3} - F_{z4}) + z \left[ (F_{x1} - F_{x2}) \sin \delta + (F_{y1} - F_{y2}) \cos \delta \right] + F_{y3} - F_{y4} \quad (8)$$

$$I_y \ddot{\phi} = l_r (F_{z3} + F_{z4}) + l_f (-F_{z3} - F_{z4}) + z \left[ (F_{x1} + F_{x2}) \sin \delta + (F_{y1} + F_{y2}) \cos \delta \right] - F_{y3} - F_{y4} \quad (9)$$

where  $l_f$  and  $l_r$  represent the distance from the COG to the front and rear axles, respectively;  $l_w$  denotes the half-track of the vehicle;  $b_f$  and  $b_r$  are the half treads of the front and rear wheels, respectively;  $\vartheta$ ,  $\phi$ , and  $\psi$  represent the roll, pitch, and yaw angles of the vehicle's body, respectively; and  $I_x$ ,  $I_y$ , and  $I_z$  are the roll, pitch, and yaw inertia of the vehicle, respectively.  $F_{z_j} = -k_s \zeta_j(\vartheta, \phi) - d_s(\dot{\zeta}_j)(\vartheta, \phi)$ , where  $\zeta_j(\vartheta, \phi)$  is the displacement of suspension  $j$  for the given roll and pitch angles of the car's body.  $F_{z_j}$  models the influence of load transfer between tires.

The rotational dynamic equation of each wheel  $j$  can be written as follows:

$$I_r \dot{\omega}_j = T_{Lj} - r_w F_{xj} \quad (10)$$

where  $I_r$  is the wheel moment of inertia around its axis,  $\omega_j$  is the angular velocity of the  $j$ th wheel,  $T_{Lj}$  is the driving torque applied on the  $j$ th wheel, and  $r_w$  is the effective rolling radius of the wheels. When the driving motor torque  $T_{Lj}$  is applied to the  $j$ th pneumatic tire, the driving force is developed at the contact patch between the tire and the road. Simultaneously, the tire tread of the contact patch and the tread within the patch are subject to compression during acceleration. The distance that the tire travels on being subjected to a driving force is less than the

distance traveled when the tire undergoes free rotation. The wheel slip ratio  $\tau_j$  of wheel  $j$ , that is, the relative motion between a driving wheel's angular velocity and the vehicle's velocity, is defined as follows:

$$\tau_j = \begin{cases} \frac{r_\omega \omega_j - v_x}{r_\omega \omega_j} & r_\omega \omega_j > v_x \text{ for acceleration} \\ \frac{r_\omega \omega_j - v_x}{r_\omega \omega_j} & r_\omega \omega_j > v_x \text{ for deceleration} \end{cases} \quad (11)$$

The lateral slip-angle  $\alpha_j$  of tire  $j$  is the angle between the wheel's orientation and its velocity. This angle can be expressed as follows:

$$\alpha_{j,f} = \delta - \frac{v_y + l_f \dot{\psi}}{v_x \pm b_f \dot{\psi}} \quad (12.a)$$

$$\alpha_{j,r} = -\frac{v_y + l_r \dot{\psi}}{v_x \pm b_r \dot{\psi}} \quad (12.b)$$

where  $f$  and  $r$  denote the front and rear wheels, respectively, and  $\delta$  is the steering angle of the front wheels.

## SIMULATION STUDY

Figure 5 displays a four-wheeler vehicle comprising the Ackermann steering system, a suspension system, wheels, and connecting rods. The Ackermann steering mechanism is a geometric arrangement of linkages in the steering of a vehicle. This mechanism was designed to ensure that the inner front wheel turns at a larger angle than the outer wheel so that the vehicle can rotate around the midpoint between the rear wheel axes while cornering. The suspension attached to the four-wheeler car is of the double-wishbone type instead of the MacPherson type because of the double-wishbone-type suspension can be used with a heavy load. The simulation parameters of the vehicle are presented in Table 2. To demonstrate the validity and stability of the proposed method for the path planner, two sets of planning simulations were conducted for lane-changing and U-turn maneuvering operations.

Table 2. Parameters of the vehicle and tires.

Symbol	Parameter	Value and Units
$M_v$	Vehicle mass	200 kg
$l_f$	Distance between the vehicle gravity center to the front axle	1.5 m
$l_r$	Distance between the vehicle gravity center to the rear axle	1.5 m
$b_f, b_r$	Half treads of the front (rear) wheels	0.9 m

$C_f$	Equivalent cornering stiffness of the front wheel	60,000 N/rad
$C_r$	Equivalent cornering stiffness of the rear wheel	40,000 N/rad
$I_x$	Moment of inertia	1000 kg·m <sup>2</sup>
$R$	Equivalent winding resistance	0.688 $\Omega$
$J$	Sum of inertia moments of the wheel and motor	7.143 kg·m <sup>2</sup>
$b$	Damping coefficient	1.0 Nm·s/rad
$L$	Equivalent inductance of the winding	0.125 H
	Maximum speed	25 m/s
	Low speed	1.5 m/s
	Near-field range	30m
	Closed-range speed ratio	0.4
	Near-range speed ratio	0.2
	Steering rewind rate	7
	Static friction coefficient	1.0

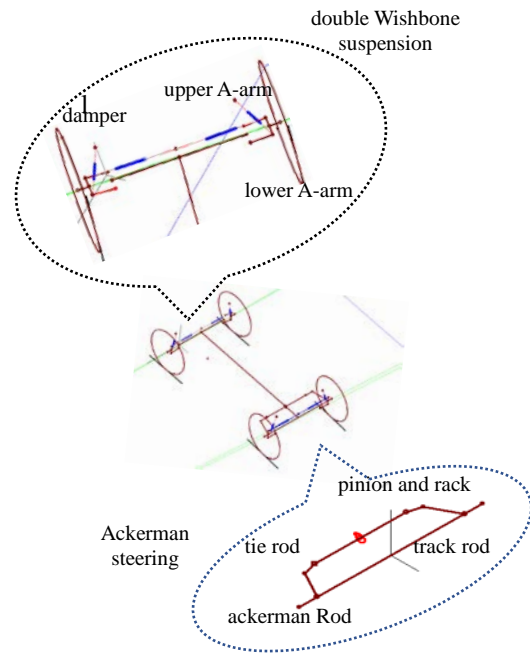


Fig. 5. Vehicle model with a steering mechanism in the front wheel and double-wishbone-type suspension in the rear wheel.

### Example 1: Lane-Change Maneuver

Figure 6 illustrates a lane-changing trajectory in the first set of simulation scenarios. A starting point of (0, 0) and target point of (100, -100) with respect to the global coordinates were specified. The yaw angle of the vehicle remains at 0° at these two points when measured from the X-axis. Figure 7 displays the graph of the target and alignment angles versus the time for the trajectory with respect to the local body coordinates. The steering command is generated using the heuristic rule table presented in Table 1. Figure 8 displays the profiles of the yaw and steering angles.

The vehicle begins from standstill at time  $t_0$ . The target angle  $\xi(t_0)$  and alignment angle  $\Delta\psi(t_0)$  are -42° and 0°, respectively. The vehicle dynamics

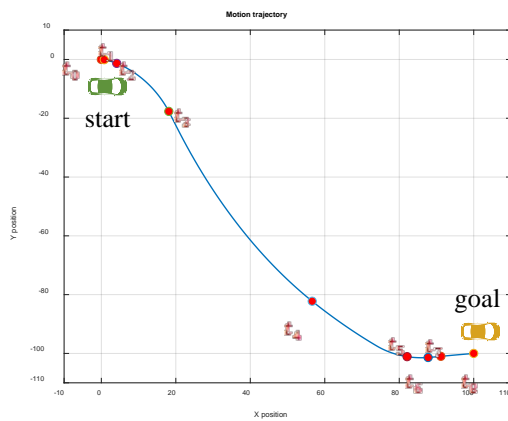


Fig. 6. Motion trajectory of the lane-changing maneuver.

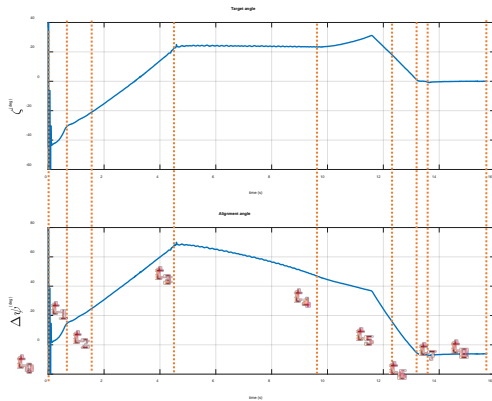


Fig. 7. Target and alignment angles in example 1.

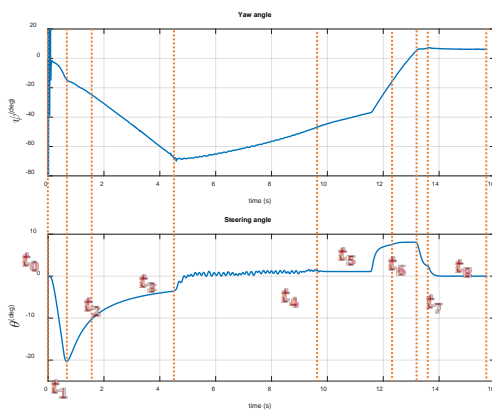


Fig. 8. Yaw angle and steering angle in example 1.

indicate that the vehicle makes reciprocal movements instantly when it begins moving. This transient transition phenomenon causes a sharp change in the yaw angle of the vehicle, as displayed in Fig. 8. From the driver’s-perspective view, the destination position is in the direction of 1:30 on the clock. Moreover, the forward direction of the vehicle is aligned with the

preset direction of the destination. According to the state (2-0) of heuristic rules listed in Table 1, the path planner issues a right turn command and decreases the steering angle  $\theta$  of the steering wheel to perform the right turn. At a  $t_1$  value of 0.6 s, as the target angle  $\xi(t_1)$  gradually changes from the direction of 1:30 on the clock and enters the region of the 12 o’clock direction, the heuristic rule states change from (2-0) to (1-0). The path planner outputs the “straight line” command and progressively rewinds the current steering angle  $\theta$  back to zero. At a  $t_2$  value of 1.69 s, the target position remains in the 12 o’clock direction. However, the alignment angle varies to the right. The heuristic state changes from (1- 0) to (1-1). The control decision results in an increment of the steering angle  $\theta$ , and the direction of the steering wheel is gradually adjusted to the left. During the time interval  $[t_2, t_3]$ , the discrete state of the target angle switches repeatedly between the 12 o’clock direction and the direction of 10:30 on the clock. The driving behavior involves the performance of the interactive “turn left” and “go straight” actions. The steering angle is near  $0^\circ$ , and the steering wheel is maintained in the center position to fine-tune the vehicle’s forward direction to the target area.

The motion trajectory can be divided into eight steps, and each step has different discrete states of target and alignment angles. According to the heuristic rules, the autonomous path planner outputs different steering commands to the steering controller. At a  $t_8$  value of 15.73 s, the vehicle enters the destination. The steering wheel remains at the center, and the yaw angle error is approximately  $6.13^\circ$ . Table 3 summarizes the eight-step actions of the lane-change trajectory based on the state changes of the heuristic rules.

Table 3. Simulation results for the lane-changing maneuver.

Symbol	Time (s)	$\psi$	$\theta$	Rule	Action
$t_0$	0	$0^\circ$	0	(2-0)	Right
$t_1$	0.60	$-12.3^\circ$	$-19.4^\circ$	(1-0)	Straight
$t_2$	1.69	$-26.4^\circ$	$-9.5^\circ$	(1-1)	Left
$t_3$	4.51	$-67.5^\circ$	$-3.6^\circ$	(1-1) (8-1)	Left Straight
$t_4$	9.81	$-45.8^\circ$	$1.1^\circ$	(8-1)	Straight
$t_5$	12.49	$-11.1^\circ$	$7.9^\circ$	(0-0)	Straight
$t_6$	13.18	$5.0^\circ$	$8.1^\circ$	(0-0) (0-1)	Straight Straight
$t_7$	13.68	$7.1^\circ$	$1.5^\circ$	(0-0)	Straight
$t_8$	15.73	$6.13^\circ$	$0.0^\circ$		

**Example 2: U-Turn Maneuver**

A starting point of (0, 0) and target point of (100, -100) with yaw angles of  $0^\circ$  and  $180^\circ$  in the opposite directions, respectively, are considered in example 2. Figure 9 displays a U-turn trajectory in the second set of simulation scenarios. The aim of a U-turn action is to maneuver a vehicle to the opposite lane. Figure 10

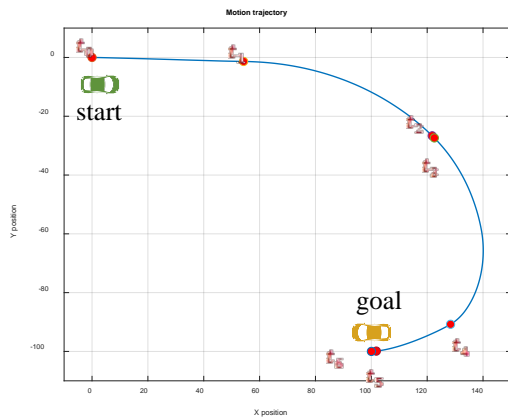


Fig. 9. Motion trajectory of the U-turn maneuver.

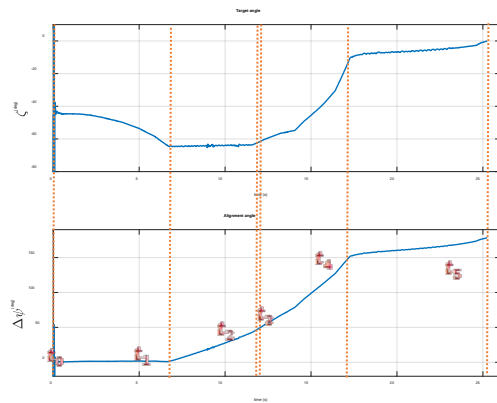


Fig. 10. Target and alignment angles in example 2.

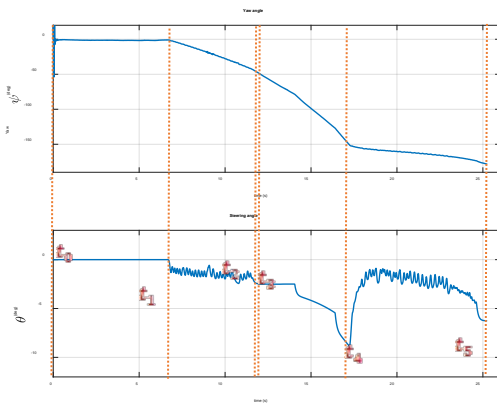


Fig. 11. Yaw angle and steering angle in example 2.

and 11 display the vehicle behaviors during a U-turn maneuver. In Figs. 10 and 11, the variations in a pair of target and alignment angles and a pair of yaw and steering angles with time are plotted, respectively. Motion planning is divided into five steps under different transition states of heuristic rules. Each step

of the path plan encodes how the vehicle behavior transitions from one point to the next. Table 4 summarizes the steering operations performed in each step.

The vehicle first travels straight ahead and then turns right. Finally, the vehicle advances straight forward into the target area, with the heading direction in the opposite direction at the starting position. The motion planner always attempts to make a forward progress. During the time intervals  $[t_1, t_2]$  and  $[t_4, t_5]$ , the steering behavior switches rapidly between the two actions of “going straight” and “turning right”. At the end of the time interval  $[t_1, t_2]$ , the steering angle has a negative value of right turn. Moreover, at the end of the interval  $[t_4, t_5]$ , the steering angle approaches zero and the steering wheel faces the center position. By combining the aforementioned five steps, the vehicle reaches the target with a yaw angle of  $5^\circ$  and steering angle of  $-6.3^\circ$  at a  $t_6$  value of 25.25 s.

Table 4. Simulation results of the U-turn maneuver.

Symbol	Time (s)	$\Psi$	$\Theta$	Rule	Action
$t_0$	0	$0^\circ$	0	(2-2)	Straight
$t_1$	6.67	$-1.01^\circ$	$0^\circ$	(2-2) (3-2)	Straight Right
$t_2$	11.59	$-43.1^\circ$	$-1.9^\circ$	(0-2)	Straight
$t_3$	11.66	$-44.0^\circ$	$-2.1^\circ$	(2-1)	Right
$t_4$	17.22	$-44.9^\circ$	$-8.8^\circ$	(2-1) (0-1)	Right Straight
$t_5$	24.67	$-11.1^\circ$	$-4.8^\circ$	(0-0)	Straight
$t_6$	25.25	$5.0^\circ$	$-6.3^\circ$		

## CONCLUSIONS

Human behavior indicates environmental awareness and self-awareness and is used to make decisions, take actions, and reach conclusions based on reasoning and inference. Environmental awareness and self-awareness are the characteristics that autonomous vehicles require to effectively plan feasible paths and operate in a dynamic operating environment. To ensure efficient operation of autonomous vehicles on roads, a novel path planner with reasoning and decision-making skills similar to humans is required for complex driving situations.

Heuristic rules can be used to plan dynamic, feasible, and comfortable trajectories while focusing on customizability. Trajectories are generated and verified through numerical calculations of the responses of the vehicle dynamics model comprising a chassis with Ackerman steering and double-wishbone suspension. The simulation results reveal the stability and accuracy of the method for planning the target motion path. The proposed method can successfully solve the tracking problem in a simple and intuitive manner and thus requires a low number of calculations and tuning processes. The

incorporation of real-time path planning with the real-world problem of static and dynamic obstacle avoidance will be considered in our future study.

## ACKNOWLEDGMENT

This work was supported by Ministry of Science and Technology, the Republic of China, under Grant No. MOST 109-2218-E-008-003 -. This manuscript was edited by Wallace Academic Editing.

## REFERENCES

- Cai, Z., Li, S., Gan, Y., Zhang, R., and Zhang, "Q. Research on complete coverage path planning algorithms based on a\* algorithms," *Open Cybern. Syst. J.* 2, 8, pp. 418–426. (2014)
- Chen, T., Chen, L., Xu, X., Cai, Y., Jiang, H., and Sun, X., "Estimation of longitudinal force and sideslip angle for intelligent four-wheel independent drive electric vehicles by observer iteration and information fusion," *Sensors*, No. 18(4), 1268. (2018).
- Dijkstra, E. W., "A note on two problems in connexion with graphs," *Numer. Math.*, No. 1(1), pp. pp. 269–271. (1959)
- Dolgov, D., Thrun, S., Montemerlo, M., and Diebel, J., "Path planning for autonomous vehicles in unknown semi-structured environments," *The International Journal of Robotics Research*, 29(5), pp. 485-501. (2010)
- González, D., Pérez, J., Milanés, V., and Nashashibi, F., "A review of motion planning techniques for automated vehicles," *IEEE Transactions on Intelligent Transportation Systems*, 17(4), pp. 1135-1145. (2015)
- Kuwata, Y., Teo, J., Fiore, G., Karaman, S., Frazzoli, E., and How, J. P., "Real-time motion planning with applications to autonomous urban driving," *IEEE Transactions on Control Systems Technology*, 17(5), pp. 1105-1118. (2009)
- Soltani, A. R., Tawfik, H., Goulermas, J. Y., & Fernando, T., "Path planning in construction sites: performance evaluation of the Dijkstra, A\*, and GA search algorithms," *Advanced engineering informatics*, 16(4), pp.291-303. (2002)
- Tavan, N., Tavan, M., and Hosseini, R., "An optimal integrated longitudinal and lateral dynamic controller development for vehicle path tracking," *Latin American Journal of Solids and Structures*, 12(6), pp. 1006-1023, (2015).
- Zhu, Q., Han, Y., Liu, P., Xiao, Y., Lu, P., and Cai, C., "Motion Planning of Autonomous Mobile Robot Using Recurrent Fuzzy Neural Network Trained by Extended Kalman

Filter," *Computational intelligence and neuroscience*, pp 1-16, (2019)

## 即時啟發式運動路徑規劃 於車輛自動駕駛應用

鄭時龍<sup>1</sup> 成維華<sup>2</sup> 王詠辰<sup>3</sup>

<sup>1</sup>龍華科技大學機械工程學系

<sup>2</sup>國立交通大學機械工程學系

<sup>3</sup>工業研究技術院 機械所

### 摘要

本文提出了一種新方法，執行四輪車輛運動路徑規劃。路徑規劃採用駕駛行為的推論啟發式方法和從駕駛員視角度獲得的相關目標方向資訊來快速，有效地產生目標路徑，而無需進行複雜的數學計算。車輛動態模型，包含有具有 Ackerman 轉向和雙叉骨懸架的底盤，來自地面接觸點的橫向和縱向力，懸架系統提供的支撐力，用於驗證車輛從起始位置到目標位置的規劃路徑運動。變換車道和 U 型轉向運動模擬顯示：本方法可即時提供可行的運動路徑。路徑規劃方法適用於不同駕駛場景，並提供動態追蹤性能與保持良好的可操縱性。它可以擴展應用於車輛即時自動導航。